Journal of Machine Engineering, 2025, Vol. 25
ISSN 1895-7595 (Print) ISSN 2391-8071 (Online)

Received: *16 Marc 2025* / Accepted: *16 April 2025* / Published online: *27 May 2025*

polishing SUS304,
ultrasonic-assisted magnetic finishing,
magnetic field distribution,
surface finishing process

Kieu Van QUANG[1], Dung Hoang TIEN[1],
Nguyen Duy TRINH[1*], Le Ngoc DUY[1],
Nguyen Van QUE[1], Pham Thi Thieu THOA[1],
Truong Van LUONG[1], Phan Tien VIET[1],
Quach Vu HIEU[1]

POLISHING OF SUS 304 STAINLESS STEEL USING A NEW MAGNETORHEOLOGICAL MACHINING TECHNOLOGY INTEGRATING ULTRASONIC VIBRATION AND MULTI-POINT ELECTROMAGNET

The increasing demand for ultra-smooth surfaces and precise control over nanoscale microstructural features in modern manufacturing has driven the development of hybrid finishing technologies. In this study, a novel Ultrasonically Assisted Magnetic Abrasive Finishing (UAMAF) method is proposed, integrating conventional Magnetic Abrasive Finishing (MAF) with high-frequency ultrasonic vibration to enhance both material removal efficiency and surface quality. A key innovation of this study is the development of a Multi-Point Electromagnet system, composed of multiple independently energized poles arranged to generate localized, intensified magnetic fields. This configuration improves the control and distribution of magnetic abrasive particles during polishing. Numerical simulations of flat, grooved, and curved head geometries revealed that the curved design (20 mm curvature height) achieved the most uniform magnetic flux. Polishing experiments on SUS 304 stainless steel confirmed that optimized process parameters such as spindle speed and DC current enabled a surface roughness (*Ra*) reduction to 15 nm after 90 minutes. The synergistic effect between ultrasonic vibrations and the multi-point magnetic control significantly improved abrasive dispersion, reduced agglomeration, and intensified micro-cutting actions at the workpiece interface. This research highlights the effectiveness of the UAMAF technique enhanced by a multi-point electromagnet system, providing new insights into hybrid finishing mechanisms. The findings hold strong potential for industrial applications in fields demanding high-precision surface integrity, such as biomedical devices, aerospace components, and optical systems.

1. INTRODUCTION

In the context of rapid technological advancement, the requirements for high-quality surface finishes in mechanical machining processes have become increasingly stringent. Surface roughness is a critical parameter that not only determines the aesthetic appearance of

[1] Hanoi University of Industry, 298 Cau Dien, Bac Tu Liem, Hanoi city, Vietnam
[*] E-mail: tiendung@haui.edu.vn
https://doi.org/10.36897/jme/204092

a product but also has a profound impact on its functional performance and service life [1, 2]. As such, enhancing surface quality after machining is pivotal to ensuring the reliability and overall performance of the final component. Among the commonly used engineering materials, SUS 304 stainless steel is particularly notable for its excellent corrosion resistance, mechanical robustness, and favourable machinability [3, 4]. Nevertheless, to fulfil the escalating standards of modern applications, it is imperative to apply advanced surface finishing techniques that can effectively exploit the intrinsic advantages of SUS 304 and guarantee its long-term operational stability.

To overcome the challenges associated with achieving high-precision surface finishes, Magnetic Abrasive Finishing (MAF) technology has emerged as a promising and extensively investigated solution. Numerous studies have demonstrated that critical process parameters—such as the cutting mode and the finishing gap play a vital role in determining the surface roughness attained during MAF operations. The optimization of these parameters not only improves surface integrity but also expands the scope of precision machining to meet the increasingly demanding requirements of modern industry [5–7]. Significant progress has been made in applying MAF to stainless steel, particularly SUS 304, which is widely used in industrial applications due to its mechanical and chemical properties [8–12]. For instance, a study conducted in 2009 reported successful polishing of SUS 304 bars using MAF, achieving a surface roughness of 0.06 μm and roundness of 0.12 μm with 1 μm diamond abrasive particles [13]. Singh et al. [14] employed Response Surface Methodology (RSM) to optimize MAF process parameters, resulting in a remarkable 92% improvement in surface finish, reducing the roughness to 0.04 μm. Lee et al. [15] introduced a two-dimensional vibration-assisted MAF technique, which enhanced polishing efficiency and achieved a 77% improvement in surface roughness, attaining a final roughness of 0.03 μm. Gill et al. [16] investigated the use of diamond-based sintered magnetic abrasives in MAF, identifying abrasive grit size as the most influential factor on surface finish, accounting for 49.49% of the effect. Collectively, these advancements have significantly contributed to the refinement of MAF process parameters and the evolution of innovative finishing techniques, thereby enhancing the surface quality of SUS 304 stainless steel in high-precision manufacturing applications.

While Magnetic Abrasive Finishing (MAF) technology has demonstrated notable success in improving surface quality, it still faces inherent limitations, including relatively low material removal rates and limited capability in rectifying surface defects [17, 18]. To address these challenges, ultrasonic technology has been integrated into surface finishing processes as an effective enhancement strategy. Ultrasonic-assisted polishing introduces high-frequency acoustic waves into the polishing medium, which accelerates material removal and facilitates the elimination of micro-defects on the workpiece surface. The underlying mechanism is primarily attributed to acoustic cavitation the formation and subsequent implosive collapse of microscopic bubbles which generates localized high-pressure shock waves. These dynamic effects contribute to dislodging surface contaminants and promoting finer surface finishes. Due to these advantages, ultrasonic-assisted technologies have gained widespread adoption across various industrial sectors, including electronics manufacturing, automotive engineering, medical device production, and general mechanical processing [19]. Recent studies have increasingly underscored the pivotal role of ultrasonic technology in enhancing the surface quality of processed materials, thereby broadening its range of applications. Ultrasonic-assisted polishing techniques have been extensively researched for enhancing the surface quality of SUS304 stainless steel and other metal materials [20–22]. Xu et al. [23] investigated the influence of ultrasonic vibrations during the turning of SUS 304 and reported more stable machining conditions and uniform chip morphology. Similarly, Cao et al. [24] proposed a hybrid method combining low-temperature chromizing with ultrasonic vibration extrusion, achieving a significant increase in surface hardness and a reduction in roughness, confirming the effectiveness of ultrasonic assistance in optimizing surface treatments. Beyond SUS304, ultrasonic-assisted electrochemical polishing has been applied to copper surfaces, improving both hydrophobicity and corrosion resistance by enhancing electrochemical reactions during polishing [25]. In the field of additive manufacturing, ultrasonic abrasive polishing has been utilized to mitigate the inherently high surface roughness of printed components by harnessing cavitation effects and the mechanical action of abrasive particles [26]. Moreover, ultrasonic-assisted abrasive waterjet polishing has demonstrated improved material removal efficiency and surface finish when applied to hard and brittle materials [27]. These studies collectively underscore the versatility and effectiveness of ultrasonic-assisted polishing techniques in achieving superior surface quality across various materials and manufacturing contexts.

In recent years, the integration of ultrasonic technology with Magnetic Abrasive Finishing (MAF) has marked a significant advancement in surface finishing, particularly for hard-to-machine and non-magnetic materials such as stainless steel [28, 29]. While ultrasonic-assisted methods improve the energy efficiency and material removal rate of traditional MAF, they still encounter limitations. Specifically, the generation of cavitation bubbles in the working fluid often lacks spatial uniformity, leading to inconsistent impact forces and localized over-wear. Moreover, the dynamics of bubble formation and collapse are not precisely controlled, which can compromise surface uniformity. To overcome these limitations, this study introduces a novel Ultrasonically Assisted Magnetic Abrasive Finishing (UAMAF) process, which combines ultrasonic vibrations with enhanced magnetic control through the use of electromagnets [30–32]. In a conventional MAF setup, electromagnets are employed to generate a magnetic field that attracts and aligns magnetic abrasive particles near the workpiece surface. The field strength and direction can be modulated by adjusting the current supplied to the coil wound around a ferromagnetic core. This configuration provides flexibility in controlling abrasive movement and pressure, essential for achieving high-quality surface finishes.

A key innovation in the present work is the development and integration of a multi-point electromagnet system. Unlike traditional electromagnets that generate a uniform field over a broad area, the multi-point electromagnet comprises multiple individually controlled magnetic poles arranged strategically across the tool head. This configuration allows for the creation of localized and intensified magnetic fields at discrete zones within the polishing area, resulting in improved guidance, concentration, and dynamic behaviour of magnetic abrasive particles. The localized control also enhances the consistency of the finishing force distribution, particularly when combined with ultrasonic cavitation effects. The effectiveness of UAMAF has been validated through numerous studies. For instance, Mulik and Pandey

[33] demonstrated the process's potential by achieving a surface roughness of 22 nm on hardened AISI 52100 steel. Subsequent research by Zhou et al. [34] extended the application to titanium components for aerospace and biomedical uses. Computational modeling and process optimization studies by Misra, Pandey, and Dixit [35] further improved parameter control and process predictability. In parallel, Shukla et al. [31] analysed the role of shearing and plowing mechanisms in sintered magnetic abrasives, highlighting their contribution to material removal dynamics. Recently, Smith et al. [36] investigated two-dimensional vibratory-assisted MAF on SUS304, emphasizing the benefits of hybrid vibration control in enhancing surface finish. Despite notable progress, challenges related to the precise coordination of ultrasonic and magnetic effects persist [37]. The proposed UAMAF system with the MPE design addresses these challenges by optimizing magnetic field distribution and enhancing abrasive particle control. As a result, this method shows significant promise for applications requiring ultra-smooth surfaces and high dimensional accuracy, particularly in high-precision industries such as aerospace, biomedical device manufacturing, and micro/nano-fabrication.

The UAMAF method presents an innovative hybrid approach for ultra-precision machining, particularly suited for non-magnetic materials such as SUS304 stainless steel. While the technique offers enhanced efficiency in material removal and surface quality, it still faces limitations related to uneven abrasive particle distribution and agglomeration caused by magnetic field inconsistencies. To address these issues, this study focuses on optimizing the magnetic field characteristics by implementing a multi-point electromagnet system specifically designed for SUS304 polishing. Various rotational speeds and DC current levels were experimentally evaluated to assess their influence on material removal performance. The results indicate that the optimized multi-point electromagnet configuration significantly improved the uniformity of magnetic field distribution, thereby achieving nano-scale surface roughness. These findings highlight the potential of Multi-Point Electromagnet enhanced UAMAF as a viable solution for future high-precision industrial applications.

2. OPERATING PRINCIPLE

2.1. EXPERIMENTAL BASIS

In this study, a direct current (DC) electromagnet was employed due to its straightforward construction and the ease with which its magnetic field can be regulated, making it a practical choice for a wide range of industrial applications [38, 39]. Given that surface polishing plays a critical role in determining the magnetic performance particularly in terms of magnetic permeability and field intensity it is imperative to select an appropriate polishing technique and precisely control process parameters to ensure optimal functionality. The electromagnet used in this setup incorporates a C45 steel core, with magnetic field direction determined according to the right-hand rule. When an electric current passes through the coil wound around the steel core, a magnetic field is generated. Magnetic flux lines emerge from the north pole, traverse the air gap, and return to the south pole. Within the steel core, these flux lines complete a closed-loop path from the south to the north pole, thereby maintaining a stable and continuous electromagnetic field.

In configurations where the C45 steel core features a cylindrical output positioned above the coil, this region acts as a flux concentration zone. If the cylindrical output functions as the north pole, the magnetic field extends outward from its surface before looping back to the south pole through the surrounding medium. Conversely, if it serves as the south pole, the field is directed inward from the external environment toward the cylinder. It is worth noting that while C45 steel is widely used, its lower magnetic permeability compared to specialized ferromagnetic materials may reduce flux concentration efficiency and contribute to magnetic losses due to scattering and hysteresis.

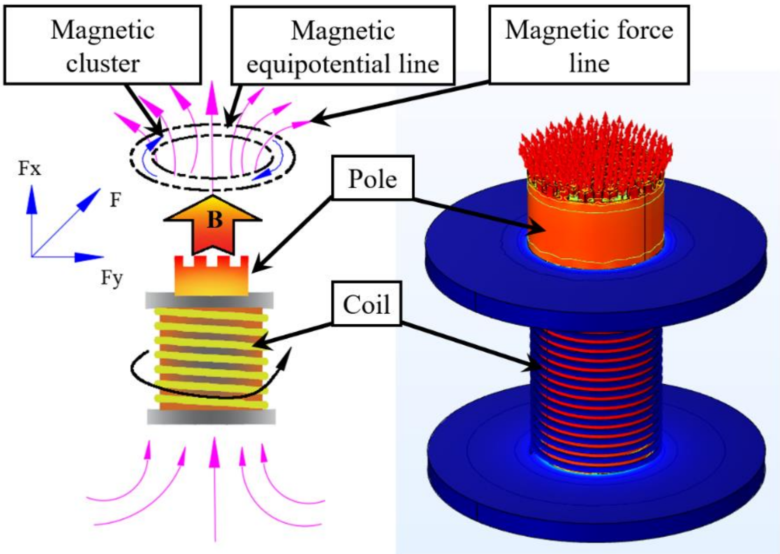

Fig. 1. Schematic of the Magnetic Force Elements within a Magnetic Field

Figure 1 illustrates the basic configuration of a system designed to generate a non-uniform magnetic field using a DC-powered electromagnet. When a direct current is applied to the coil, a stable magnetic field is established, with the magnetic flux density reaching its maximum at the two magnetic poles. The magnetic flux lines are visibly curved, especially near the poles [40]. An object placed on a tray between these poles experiences an uneven magnetic force due to the irregular field distribution, represented by the F_x and F_y vectors [41–44]. Additionally, the equipotential lines highlight the variation in magnetic potential across different spatial points. This principle is widely utilized in electromagnetic devices such as DC motors, DC generators, and magnetic field measurement instruments.

$$F_x = V.\chi.\mu_0.H.\frac{dH}{dx} \tag{1}$$

$$F_y = V.\chi.\mu_0.H.\frac{dH}{dy} \tag{2}$$

Where, V represents the volume of the magnetic particles, χ denotes the magnetic susceptibility, μ_0 indicates the permeability of free space, and H corresponds to the magnetic field intensity.

When a direct current flows through the coil of a fixed electromagnet, it produces a stable magnetic field characterized by well-defined flux lines and a constant intensity. The resulting magnetic force acts on magnetic materials with uniform magnitude and direction. Although the electromagnet itself remains stationary, this force can be utilized to secure magnetic materials, generate pulling or pushing actions, or serve as a foundation for magnetic sensor devices. Owing to the consistent nature of its magnetic field and force, the electromagnet is a critical component in a wide range of industrial and scientific applications, including magnetic polishing technologies.

2.2. MECHANISM OF ACTION

Figure 2 demonstrates the working concept of the MAF process that employs a dynamic magnetic field. In this setup, a tray filled with a composite magnetic slurry-comprising iron powder, abrasive particles, and a liquid medium is positioned between the workpiece and the magnetic poles. When an alternating current passes through the coil, the resulting fluctuating magnetic field induces an attractive force at the poles, causing the iron particles to cluster together near these regions. Abrasive particles, mixed with the iron particles, are consequently drawn into this magnetic aggregation situated between the tray and the workpiece. The combined effect of rotational and axial motions of the magnetic poles creates convective friction forces that act directly on the workpiece surface. These friction forces, together with the oscillating magnetic field, efficiently remove excess material, leading to a high-precision surface finish. This mechanism optimizes the machining process by leveraging the interplay between friction, magnetic forces, and mechanical motion.

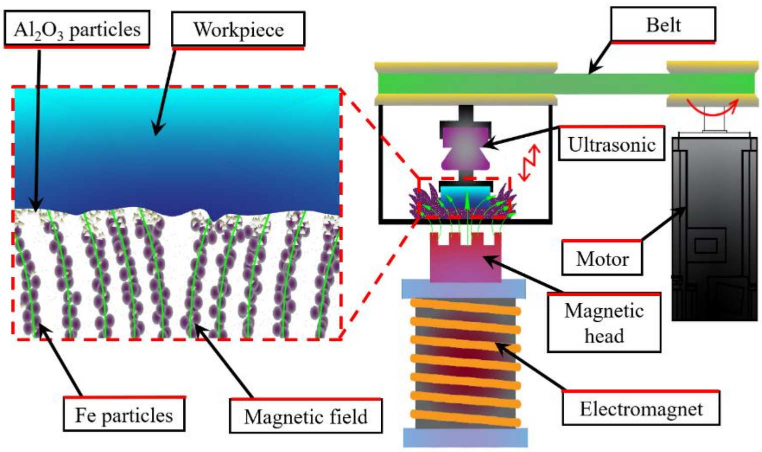

Fig. 2. The ultrasonic-assisted magnetic abrasive finishing (UAMAF)

3. INVESTIGATE THE MAGNETIC FIELD'S ATTRIBUTES

As shown in Fig. 3, the experimental setup used for magnetic field measurement is presented alongside the corresponding magnetic flux density distribution within the machining zone. The measurements were conducted using the KT-101 Gaussmeter (Kaituo

Instruments, China), a handheld device with a measurement accuracy of ±0.1 mT. This instrument enabled accurate detection of the magnetic field strength across different points within the working area. A 3 mm-thick plastic plate is fixed on a support column and marked at 3 mm intervals from the centre outward, allowing the probe to contact the plate surface for measurement. The results indicate a peak flux density of about 120 mT at $x = \pm 20$ mm, decreasing to around 80 mT at the center ($x = 0$), and further dropping to roughly 70 mT at the outer edge ($x = \pm 50$ mm). This distribution suggests that the magnetic force acting on the workpiece is strongest near $x = \pm 20$ mm, while the periphery exhibits a broader spread of magnetic particles. These findings provide a crucial basis for optimizing pole design and working distance to enhance the overall efficiency of electromagnetic machining processes.

Simulations confirm that the optimal electromagnet head configuration for high-intensity magnetic fields in machining can be identified by evaluating four distinct head designs. Each geometry's magnetic flux distribution, field strength, and focusing capability were analysed under realistic operating conditions. The resulting data establish a scientific basis for selecting the most suitable electromagnet head, thereby enhancing machining efficiency and improving post-processing surface quality. Figure 4 illustrates the electromagnet magnitudes corresponding to each pole tip shape.

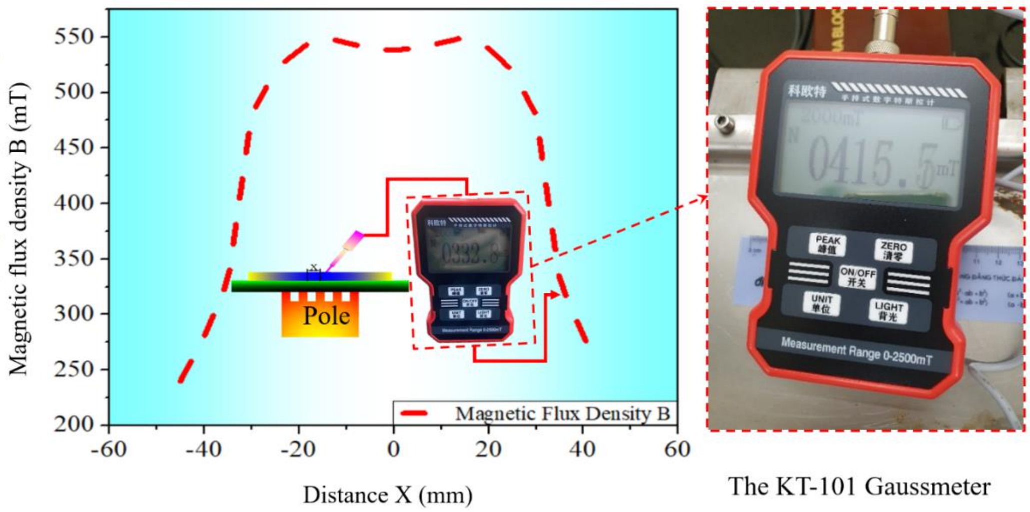

Fig. 3. Experimental setup for magnetic field measurement using the KT-101 Gaussmeter and field visualization system

Based on the magnetic field distribution charts for four different magnet pole shapes, each design exhibits a distinct peak magnetic field. For instance, the Concave shape (blue line) reaches the highest level at approximately 180 mT when the displacement is about 2 mm. The Conical shape (green line) follows with a peak around 165 mT, while the Truncated shape (red line) achieves roughly 160 mT. In contrast, the Flat groove shape (pink line) has a maximum of about 150 mT. Although the Flat groove's peak intensity is lower, it offers significant advantages in terms of uniformity and stability of the magnetic field distribution. In machining processes, maintaining a uniform magnetic field is critical for directing abrasive particles along a specific path to achieve optimal material removal. The stable magnetic field provided by the Flat groove design allows for more precise control of particle movement, reducing the irregular oscillations that can occur with designs that exhibit high but uneven field intensities. Consequently, this results in a consistently smooth surface finish and optimizes the polishing process. Even though its maximum field strength is lower than that of the Concave shape, the Flat groove is preferred in applications where high abrasive efficiency and superior surface quality are essential.

To further understand the impact of pole shape on magnetic properties, the authors conducted a detailed analysis of the geometric parameters of each design. Fig. 5 illustrates the differences in magnetic field intensity among various attachment configurations, including convex, concave, and flat surfaces. This analysis is crucial for identifying the optimal design, thereby enhancing machining performance and improving the overall quality of the finished product.

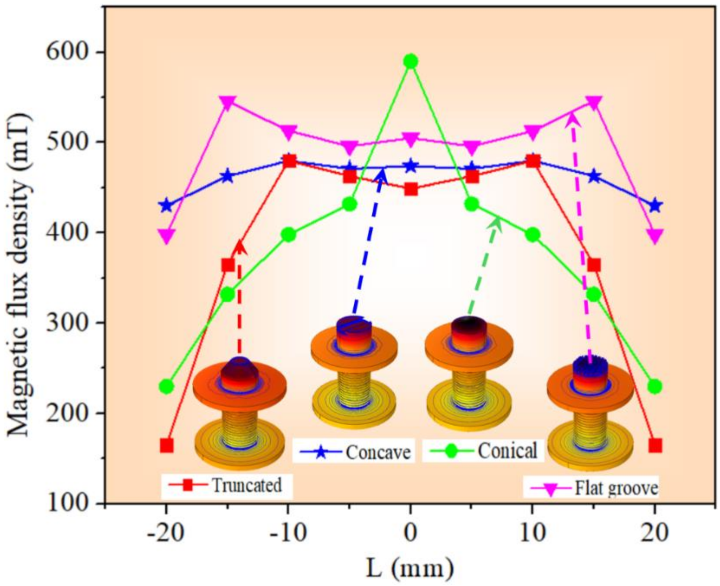

Fig. 4. Magnetic Field Magnitude of the Electromagnets

Based on the study, the maximum magnetic flux density values for the three configurations are 1.75 T for Fig. 5a, 1.83 T for Fig. 5b, and 1.89 T for Fig. 5c. While all three setups generate a magnetic field strong enough for effective machining, Fig. 5c clearly outperforms the others by achieving the highest concentration of magnetic flux at 1.89 T. Magnetic flux contours were used to visualize the spatial distribution of the field in the machining area. In Fig. 5c shown the flux lines are densest in the central region, indicating a superior concentration compared to Figs. 5a and 5b. This concentrated and uniform magnetic field creates an optimal machining zone that enhances both polishing and grinding processes. Additionally, arrow line diagrams provide detailed information on the direction and intensity of the interactions among the electromagnets.

In Fig. 5c, the arrows are not only more numerous but also larger, suggesting stronger magnetic interactions. Their consistent orientation implies that the magnetic field is tightly controlled, which helps maintain stable movement of abrasive particles during processing. These results confirm that the convex spherical configuration in Fig. 5c not only achieves a high magnetic field intensity but also ensures an even field distribution, resulting in optimal processing efficiency. In summary, the combined evidence from the flux contours and arrow line diagrams indicates that the configuration in Fig. 5c, with a peak of 1.89 T, is the optimal choice for the electromagnet system in the polishing process. Its ability to provide a highly concentrated yet uniform magnetic field significantly enhances grinding efficiency and surface quality, meeting the rigorous demands of modern industrial manufacturing.

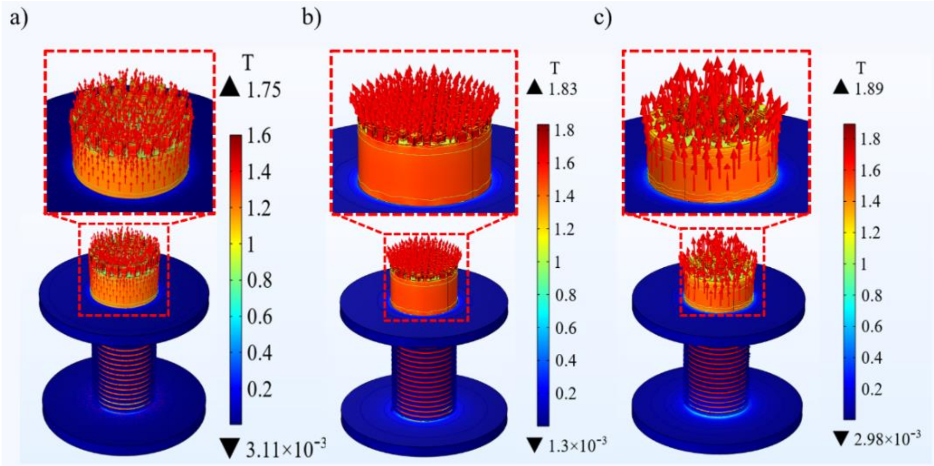

Fig. 5. Magnetic Field Intensity of Different Pole Types: a) Concave, b) Flat, c) Convex

To determine the optimal convex configuration for generating a high-intensity magnetic field, the study measured and analysed the magnetic field across various curvature levels. The electromagnet head was designed with partitioning grooves and varying curvature amplitudes to evaluate the impact of head shape on both field intensity and distribution in the processing area. As shown in Fig. 6, the density of flux lines and the corresponding magnetic field intensity on the workpiece surface are visually presented, reflecting the field's variation with respect to the electromagnet head geometry. Through quantitative analysis and comparisons among different designs, the study identified the optimal configuration to maximize machining performance. The results indicate that this configuration not only enhances the concentration of the magnetic field but also maintains a high intensity in the processing zone without significantly increasing the size or power of the electromagnet system.

Experimental results that varied the electromagnet head's curvature from 0 mm to 30 mm form the basis of Fig. 6, which illustrates the relationship between curvature height and magnetic flux density in the machining zone. The horizontal axis shows the curvature height (0–30 mm), and the vertical axis displays the magnetic flux density (in mT). The graph clearly shows that as the curvature height increases from below 10 mm to 20 mm, the magnetic flux density rises significantly and then gradually decreases. Our measurements indicate that the maximum magnetic flux density occurs at a curvature height of 20 mm, confirming that this curvature optimally concentrates the magnetic field in the polishing area (approximately 40 mm in diameter). The results demonstrate that a 20 mm curvature not only maximizes the magnetic flux density but also optimizes its distribution within the machining zone, which in turn enhances the efficiency of both polishing and grinding processes. Furthermore, the design maintains a high magnetic flux density without requiring a significant increase in the size or power of the electromagnet system, thereby reducing costs and ensuring superior surface quality during machining.

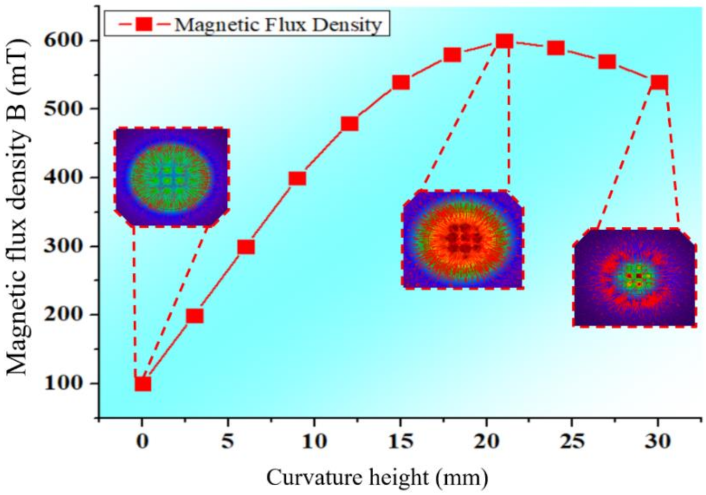

Fig. 6. Optimal Curvature of Convex Pole Tip

4. MATERIAL REMOVAL CAPABILITY IN THE UAMAF PROCESS

Ultrasonic-assisted magnetic abrasive finishing (UAMAF) is an advanced process that combines magnetic abrasive finishing (MAF) with ultrasonic oscillation (UA) to optimize machining performance, enhance surface quality, and increase the material removal rate (MRR) [45, 46]. In this method, the magnetic field directs and controls the motion of abrasive particles [47, 48], while ultrasonic vibrations supply additional energy to boost their kinetic energy and cutting capability [49]. The motion of abrasive particles in the UAMAF process can be represented by the following integral equation [50]:

$$\delta_{i2} = \int_0^t A_{i2} S_{i2}(t)dt \tag{3}$$

In this equation, δ_{i2} represents the displacement amplitude of the abrasive particles over time (mm), A_{i2} denotes the overall oscillation amplitude of the particles, and $S_{i2}(t)$ indicates the temporal variation in the oscillation.

$$\delta_{i2}(t) = d_4 a_2 \sin^{-1}\left(\frac{da_i}{dt}\right) - d_i\left(\frac{da_4}{dt^2}\right) + \sqrt{\left(\omega_r \cos(\omega t) + 2\pi fA\cos(2\pi ft)\right)^2 + \left(\omega_r \sin(\omega t) + 2\pi fA\sin(2\pi ft)\right)^2} \tag{4}$$

Here, d_4 and d_i represent geometric parameters associated with the movement trajectory of abrasive particles, while a_2 and a_4 are influenced by the ultrasonic vibration system. When accounting for the combined effects of the magnetic field and ultrasonic vibration, the instantaneous velocity of the abrasive particles can be expressed as:

$$v_m = \sqrt{\left(\omega_r \cos(\omega t) + 2\pi fA\cos(2\pi ft)^2 + \omega_r \sin(\omega t) + 2\pi fA\sin(2\pi ft)^2\right)} \tag{5}$$

where ω_r represents the angular velocity of the magnetic table (rad/s), f is the frequency of ultrasonic vibration (*Hz*), and A is the amplitude of ultrasonic vibration (mm). Based on the above equation, the trajectory of the abrasive particles can be described by the following differential equation:

$$\frac{d^2x}{dt^2}+\omega_r^2 x=-2\pi fA\sin\left(2\pi ft\right) \tag{4}$$

$$\frac{d^2y}{dt^2}+\omega_r^2 y=2\pi fA\cos\left(2\pi ft\right) \tag{5}$$

The material removal rate (MRR) in UAMAF depends on various factors, including the amplitude of ultrasonic vibration, magnetic field intensity, tool feed rate, and the impact force of abrasive particles. The empirical equation describing MRR is given as:

$$MRR=K.B^n.A_{UA}^m.v^p.F^q \tag{6}$$

where K represents the empirical coefficient, B denotes the magnetic field intensity (T), A_{UA} stands for the amplitude of ultrasonic vibration, v is the tool feed rate (mm/s), and F corresponds to the impact force of the abrasive particles (N). By substituting the expression for the impact force F_c, we derive:

$$MRR=K.B^n.A_{UA}^{m+3q}.v^p.f_{UA}^{2q} \tag{7}$$

This demonstrates that MRR rises as the amplitude and frequency of ultrasonic vibration increase, while also being affected by factors such as the magnetic table's rotational speed and the abrasive particles' cutting pressure. The cutting force of abrasive particles in the UAMAF process can be determined using the following equation:

$$F_c=\frac{1}{2}\rho\left(4\pi^2.f_{UA}^2.A_{UA}^3\right) \tag{8}$$

In this equation, ρ represents the density of the abrasive slurry (kg/m^3). The relationship indicates that the cutting force is proportional to the cube of the oscillation amplitude and the square of the ultrasonic frequency. In other words, increasing the amplitude and frequency results in a higher force acting on the workpiece surface, thereby improving the efficiency of the material removal process. Furthermore, the surface roughness (*Ra*) after machining can be modeled as follows:

$$Ra=\frac{\rho\left(4\pi^2.f_{UA}^2.A_{UA}^3\right)}{4A_c.E} \tag{9}$$

In this equation, A_c represents the contact area between the abrasive particles and the workpiece surface, while E denotes the elastic modulus of the material (Pa). The equation indicates that an increase in both the amplitude and frequency of ultrasonic oscillations results in a decrease in surface roughness, attributable to the combined effects of magnetic abrasive motion and the ultrasonic impingement effect. However, if the tool's feed rate is excessively high, the surface roughness may increase due to the sliding action of the abrasive particles on the workpiece surface.

5. EXPERIMENTS AND DISCUSSION

The model shown in the image (Fig. 7) represents a surface finishing system that integrates ultrasonic technology with a magnetic field, designed to optimize the polishing process for hard-to-machine materials. The system consists of several essential components, each serving a specific function. The central controller regulates and adjusts the operational parameters, while the AC to DC converter converts alternating current into direct current, ensuring a stable power supply for the electromagnetic components. The ultrasonic adjustment unit fine-tunes the frequency and amplitude of the ultrasonic head, generating high-frequency vibrations that enhance the polishing process. Additionally, the speed controller regulates the motor's rotation speed to maintain optimal machining conditions.

Table 1 summarizes the key experimental parameters and configuration settings employed during the polishing process. The selected workpiece material was SUS 304 stainless steel, with dimensions of 40 mm × 30 mm × 10 mm. This material was chosen due to its widespread use in precision engineering, owing to its excellent mechanical properties and corrosion resistance. The rotational speed of the polishing drum was systematically varied from 100 to 800 rpm to investigate its influence on the material removal efficiency and resulting surface finish. A cutting pass speed of 300 mm/s was maintained to ensure consistent contact between the magnetic abrasive particles and the workpiece surface throughout the experiments. The working distance, defined as the vertical gap between the electromagnet head and the surface of the workpiece, was precisely set to 0.8 mm. This distance was optimized to ensure effective magnetic field penetration and stable abrasive particle alignment in the machining zone. The MAF used in this study was composed of 15 wt.% Al_2O_3 abrasive particles, 45 wt.% Fe magnetic particles, and 40 wt.% deionized water as the carrier medium. This formulation was selected to simultaneously achieve effective mechanical abrasion and a stable, responsive magnetic field structure under applied current.

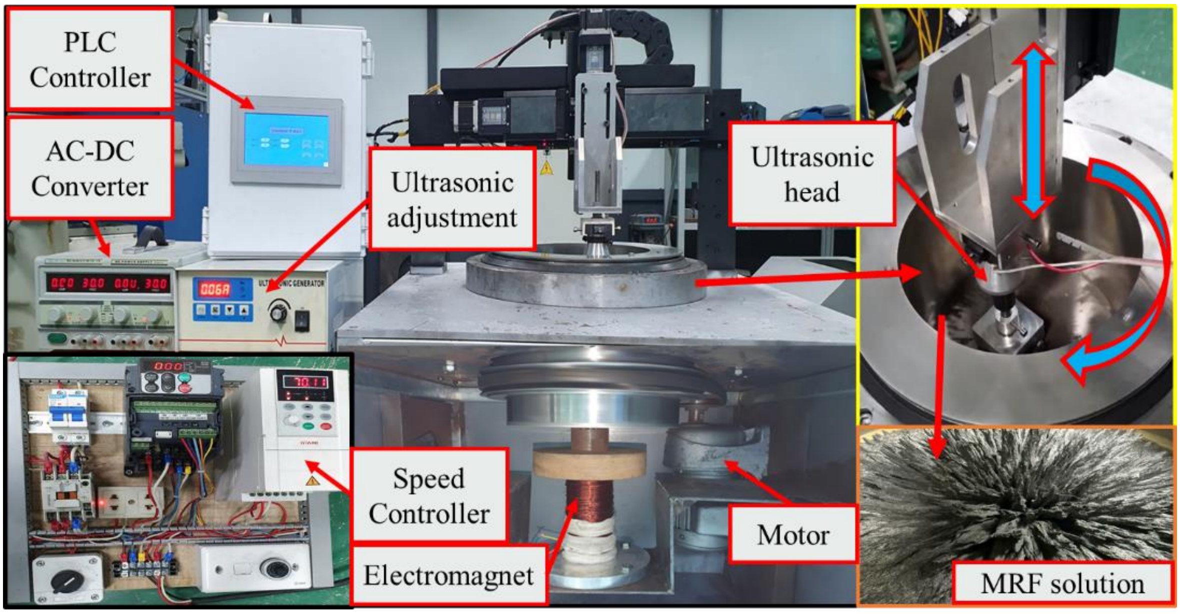

Fig. 7. Experimental setup

An electric current of 3 A was supplied to the electromagnet to generate a strong and consistent magnetic field. The electromagnet head was designed with an arc-grooved shape, which was found to enhance magnetic flux concentration and facilitate controlled movement of abrasive particles within the polishing zone. Each polishing experiment was conducted over a fixed duration of 90 minutes, a parameter determined from preliminary testing as optimal for achieving significant surface roughness reduction without inducing excessive material removal.

The electromagnet generates a magnetic field that activates and directs the movement of magnetic abrasive particles within the processing fluid, improving surface finishing efficiency. The right section of the image illustrates the system's operating principle. In this setup, the ultrasonic head, combined with a rotating magnetic field, induces intense movement of the abrasive particles, enhancing their cutting efficiency and improving surface smoothness. The magnified view below shows the concentration of magnetic abrasive particles around the tool head, clearly demonstrating the detailed polishing mechanism. By combining ultrasonic vibrations with a magnetic field, this system effectively machines high-hardness materials such as alloys and stainless steel, achieving a nanometer-level surface finish that meets the stringent requirements of precision manufacturing.

Table 1. Parameters of the experiment

Parameters	Value	Material	Note
Workpiece		Inox SUS 304	Size: 40 mm x 30 mm×10 mm
Rotation speed	100–800 rpm		
Cutting passes	300 mm/s		
Working distance	0.8 mm		
MRF fluid mixture		Al_2O_3:15%, Fe: 45%	Deionized water: 40%
Amperage	3A		
Extremely magnetic shape	Arc groove		
Processing time	90 min		

5.1. INFLUENCE OF ROTATIONAL SPEED

The experimental results presented in Fig. 8 illustrate the correlation between spindle speed, MRR and surface roughness (*Ra*) in the ultrasonic-assisted magnetic polishing process. With regard to MRR, the data indicate an increasing trend as spindle speed rises from the lowest value to approximately 500 rpm. This can be explained by the fact that a higher spindle speed generates more frequent collisions between the magnetic abrasive particles and the workpiece surface, thereby enhancing material removal efficiency. However, beyond 500 rpm, MRR starts to decline. This reduction may result from the excessive centrifugal force causing the abrasive particles to be ejected from the working zone or reducing the interaction time between the particles and the workpiece surface. Concerning surface roughness (*Ra*), the results demonstrate a decreasing trend as spindle speed increases from the lowest value to around 300 rpm. This improvement is likely due to the more uniform distribution of magnetic abrasive particles on the workpiece surface, which enhances the polishing effect. However, when the spindle speed exceeds 300 rpm, *Ra* begins to increase again. This deterioration in surface quality may be attributed to excessive particle movement at high speeds, leading to unwanted scratches or surface damage.

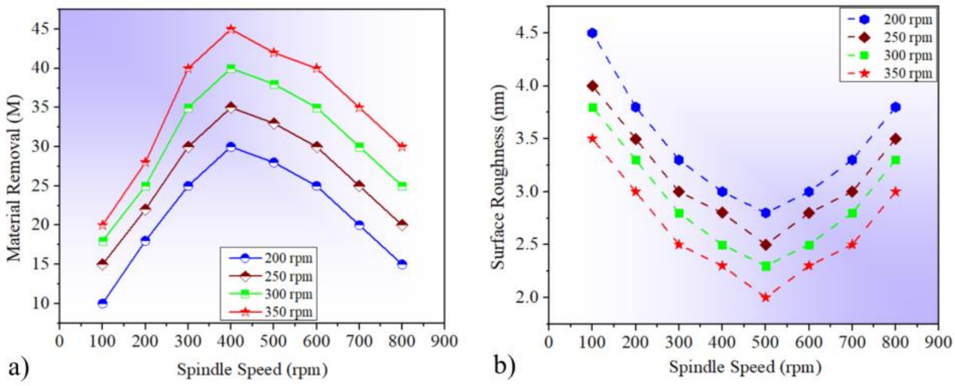

Fig. 8. Effect of Speed on Material Removal Rate: a) Material removal at different spindle speeds; b) Surface roughness at different spindle speeds

These findings suggest that an optimal spindle speed exists, balancing material removal efficiency and surface quality. Exceeding this optimal speed may lead to adverse effects, highlighting the importance of precise parameter control in advanced polishing processes. Overall, the experimental results indicate that spindle speed has a significant impact on both MRR and Ra in the ultrasonic-assisted magnetic polishing process. There exists an optimal spindle speed range (approximately 300–500 rpm) that achieves both high MRR and low Ra. This speed range should be specifically determined for each application and workpiece material to ensure optimal performance and surface quality.

5.2. EFFECTS OF CURRENT INTENSITY

In metal machining processes, electric current intensity is a critical parameter that significantly affects both the material removal rate (MRR) and surface roughness (*Ra*). Within the context of MAF, the current supplied to the direct current (DC) electromagnet directly determines the strength of the generated magnetic field, thereby influencing the behaviour and effectiveness of the abrasive particles. As the current increases, the magnetic field intensity correspondingly rises, enhancing the force used to retain and guide abrasive particles during the finishing process. At low current levels, the magnetic field is insufficiently strong to maintain stable control over the abrasive particles, resulting in irregular particle motion and inconsistent contact with the workpiece surface. This leads to elevated surface roughness and suboptimal surface quality.

Conversely, when the current reaches an optimal level, the magnetic field becomes adequately strong to uniformly stabilize the abrasive particles without imposing excessive constraints. Under these conditions, the abrasives are able to interact effectively and uniformly with the workpiece surface, enhancing cutting and polishing performance. As a result, a highly smooth and reflective surface finish can be achieved. However, if the current exceeds the optimal threshold, the magnetic field may become excessively strong, restricting the dynamic movement of abrasive particles. This over-constraining effect can decrease the efficiency of material removal and increase localized heat generation, potentially leading to surface damage or equipment wear. The MRR, defined as the volume of material removed per unit time, and surface roughness, a measure of surface texture, are thus both closely linked to current intensity. The relationship between these parameters and varying current levels is illustrated in Fig. 9, highlighting the importance of optimizing current input to achieve the desired surface characteristics and machining efficiency.

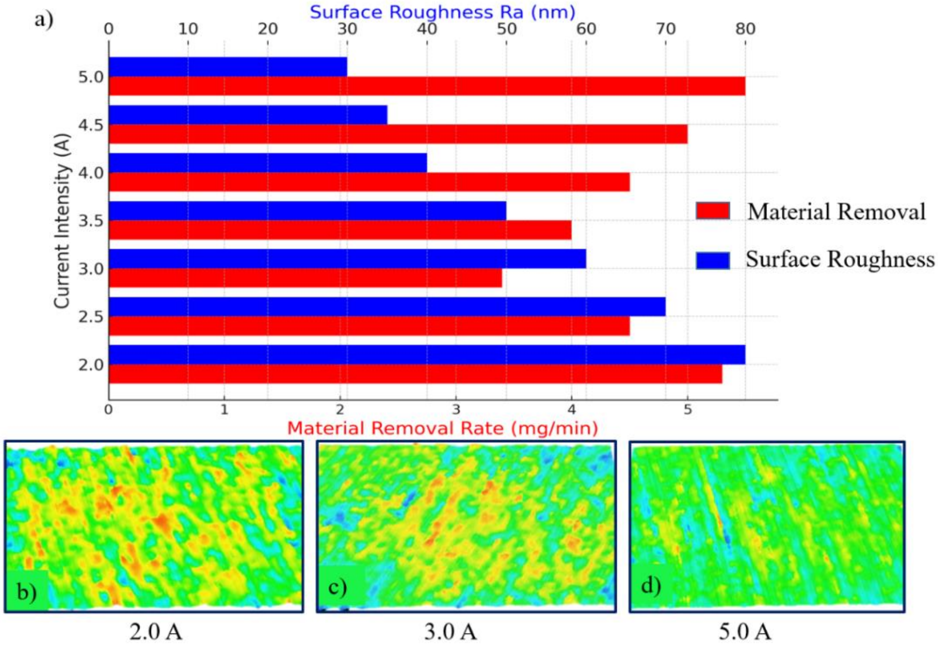

Fig. 9. Electric current affects the ability to remove materials

Based on the analysis presented in Fig. 9, a current intensity of 3.0 A was identified as the optimal machining condition, offering a favourable balance between surface quality and material removal efficiency. As shown in Fig. 9a, increasing the current from 2.0 A to 3.0 A leads to a marked reduction in surface roughness (indicated by the blue curve), reflecting a notable improvement in surface smoothness. However, when the current reaches 5.0 A, the surface roughness begins to increase, likely due to excessive material removal that compromises surface integrity. Simultaneously, the material removal rate (MRR), represented by the red curve, increases with higher current intensity. Nonetheless, at 5.0 A, the elevated MRR appears to induce surface defects such as pitting and localized deformation, thereby reducing process controllability and surface finish quality. These trends are further supported by surface morphology images shown in Figs. 9b–9d. At 2.0 A (Fig. 9b), the surface remains relatively rough, suggesting insufficient polishing action. In contrast, at 3.0 A (Fig. 9c), a uniform and significantly smoother surface is observed, indicating effective polishing. However, at 5.0 A (Fig. 9d), signs of over-processing emerge, characterized by localized roughness and possible surface damage. Taken together, both quantitative data and qualitative surface observations confirm that a current of 3.0 A provides optimal conditions for achieving high-quality surface finishes while maintaining process stability and minimizing adverse effects associated with excessive erosion.

5.3. THE IMPACT OF POLISHING DISTANCE

The two graphs present experimental results comparing surface roughness at varying polishing distances. Figure 10a) illustrates the evolution of surface roughness over time for different polishing distances. A rapid decrease in surface roughness is observed during the initial 50 minutes, corresponding to the coarse polishing stage, where substantial material removal occurs. Beyond approximately 60 minutes, the reduction rate diminishes and eventually stabilizes, indicating a transition to the fine polishing phase characterized by minimal material removal and surface refinement. At polishing distances of 0.6 mm and 0.8 mm, surface roughness reaches approximately 20 nm, indicating superior surface quality. This improvement can be attributed to the stronger magnetic field at these distances, which enhances material removal efficiency and optimizes the interaction between magnetic forces and the workpiece surface. In contrast, as the polishing distance increases to 1.0 mm and 1.2 mm, the weakening of the magnetic field reduces the effectiveness of the polishing process, causing abrasive particles to make inconsistent contact with the surface and resulting in higher final roughness values. Figure 10b) compares different surface roughness parameters (R_a, R_q, R_z, R_t) at various polishing distances. As the distance increases from 0.6 mm to 1.4 mm, all roughness parameters exhibit an upward trend, with R_z and R_t experiencing the most significant increase, indicating greater surface irregularities. This trend occurs because a larger polishing distance weakens the magnetic field, reducing its ability to confine and compress abrasive particles within the machining zone. As a result, the particles become unevenly dispersed, leading to lower material removal efficiency and a less uniform surface finish.

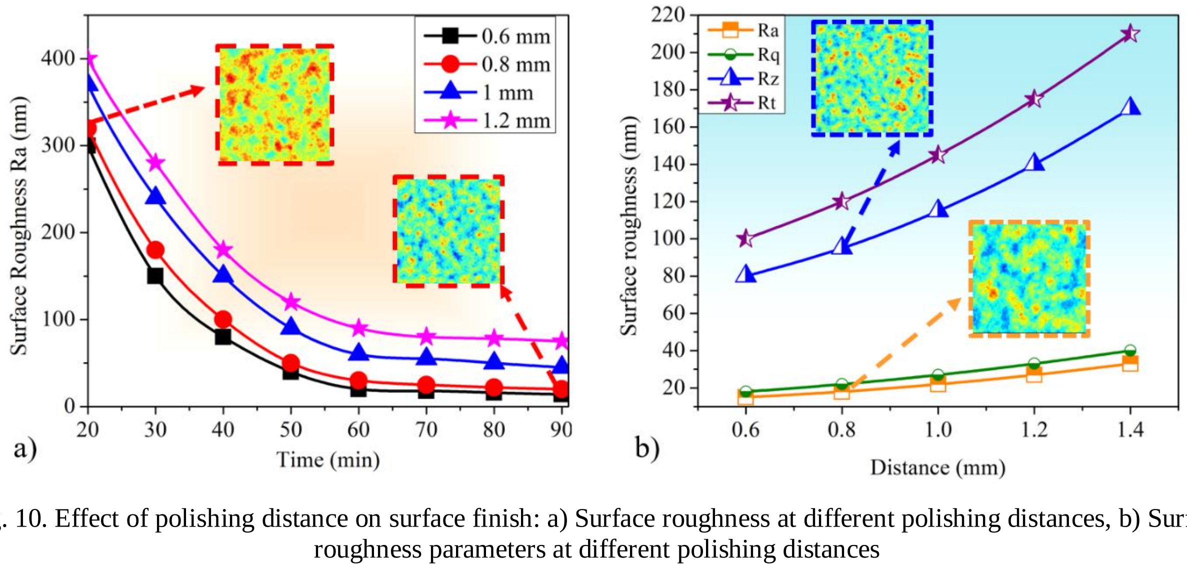

Fig. 10. Effect of polishing distance on surface finish: a) Surface roughness at different polishing distances, b) Surface roughness parameters at different polishing distances

Based on these findings, a polishing distance of 0.8 mm is identified as the optimal parameter for further investigation. This distance not only achieves lower surface roughness compared to larger distances but also maintains a sufficiently strong magnetic field to sustain polishing efficiency. Furthermore, it allows for better control over the material removal process, ensuring a smoother and more uniform surface finish. Additionally, it mitigates the risk of excessive magnetic forces, as observed at 0.6 mm, which could cause material buildup or compromise the precision of the polished surface. Therefore, a polishing distance of 0.8 mm represents the best balance between polishing efficiency and surface quality, ensuring greater process stability and consistency.

Surface roughness is the most critical parameter in the polishing study of SUS304 material, as it determines both the surface quality and the functional performance of the machined component. In this study, the effect of polishing distance on surface roughness was analysed to identify the optimal conditions for achieving a smooth and uniform surface. Furthermore, the images in Fig. 11 reinforce this conclusion by illustrating the significant improvement in surface quality between the two polished metal samples.

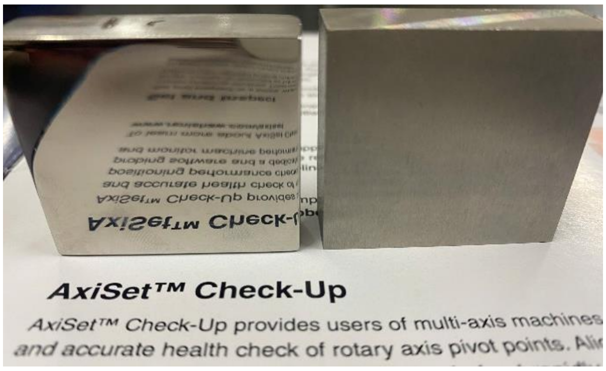

Fig. 11. SUS304 workpiece after completing the polishing process

Figure 11 presents a clear comparison of surface roughness between two metallic specimens following the machining process, effectively demonstrating the polishing technique's efficacy in enhancing surface quality. The specimen on the left exhibits a smooth, glossy surface with high reflectivity, as evidenced by the legible printed text beneath it. This indicates a substantial reduction in surface roughness potentially reaching the nanometer scale suggesting the successful removal of residual machining marks and the formation of a highly refined surface. Such improvements not only enhance visual appearance but also contribute to reduced friction, lower risk of contamination, and extended service life. In contrast, the specimen on the right shows a matte, non-reflective surface, indicative of comparatively high surface roughness. This may result from the absence of post-processing or insufficient polishing, which prevents the attainment of an ultra-smooth finish. Elevated surface roughness increases microscopic surface irregularities, leading to greater contact area and friction factors that can adversely affect the performance and longevity of mechanical components. Furthermore, rough surfaces are unsuitable for high-precision applications such as optical systems, precision mechanical assemblies, and mold fabrication in advanced manufacturing contexts.

The observed differences between the two material specimens underscore the critical importance of surface polishing in machining processes. Achieving a smoother surface finish not only enhances the functional performance of components but also extends their operational lifespan by minimizing wear and mitigating friction-induced damage, particularly under demanding working conditions. This is of particular significance in high-precision industries such as electronic component manufacturing, precision engineering, mold fabrication, and semiconductor processing where even slight variations in surface roughness at the micrometer level can markedly affect product quality, reliability, and overall performance.

5. CONCLUSION

This study presents a systematic investigation of the UAMAF technique as a novel hybrid surface finishing approach designed to overcome the inherent limitations of conventional methods, particularly in the context of SUS 304 stainless steel a material characterized by high strength, excellent corrosion resistance, and low machinability. By integrating magnetic field-guided abrasive control with high-frequency ultrasonic vibrations, the UAMAF process significantly improves both material removal efficiency and the uniformity of surface finishing. In this method, the magnetic field governs the spatial distribution and directional motion of abrasive and magnetic particles, while ultrasonic excitation enhances particle dispersion, mitigates agglomeration, and facilitates intensified micro-cutting actions at the workpiece interface. This synergistic mechanism minimizes surface defects such as waviness and micro-scratches, thereby enabling high-quality polishing. The experimental findings demonstrate that the UAMAF technique is capable of achieving surface roughness at the nanometer scale, indicating its strong potential for deployment in high-precision manufacturing sectors. The principal conclusions drawn from the study are summarized as follows:

- A comprehensive set of experiments was performed utilizing three distinct geometries of electromagnet heads: flat, grooved, and curved with the curved configuration exhibiting a curvature height of 20 mm. Among these, the curved design produced the most uniform magnetic flux distribution within the machining zone, which in turn significantly enhanced the stability of abrasive particle motion and contributed to the achievement of superior surface quality.
- After 90 minutes of processing, the surface roughness (Ra) of SUS 304 was successfully reduced to 15 nm. This remarkable improvement over conventional magnetic abrasive finishing (MAF) techniques highlights the enhanced performance capabilities of the UAMAF method in delivering ultra-smooth surfaces on materials with high hardness and corrosion resistance.
- Process parameters were systematically optimized by varying the spindle rotational speed within the range of 100 to 800 rpm and supplying a constant current of 3 A to the DC electromagnet. These adjustments enabled effective tuning of the magnetic field strength and abrasive flow dynamics, thereby maximizing material removal rates while preserving nanoscale surface integrity.
- An optimal working gap of 0.8 mm between the electromagnet and the workpiece was established through experimental analysis. This specific distance was found to provide a balance between magnetic field effectiveness and controlled abrasive flow, ensuring consistent polishing performance throughout the machining zone.

– In contrast to prior studies that focused exclusively on magnetic abrasive mechanisms, this research demonstrates the benefits of integrating ultrasonic vibrations. The inclusion of high-frequency mechanical oscillations not only improves the dispersion and trajectory of abrasive particles but also enhances the uniformity and repeatability of the finishing process particularly for challenging workpiece materials such as stainless steel.

Overall, the study validates the UAMAF approach as an innovative, efficient, and industrially viable surface finishing technology. Furthermore, the findings establish a foundation for future investigations into multi-physics coupling effects and the development of intelligent, adaptive control strategies for hybrid finishing systems.

NOMENCLATURE

UAMAF	Ultrasonically Assisted Magnetic Abrasive Finishing	V	Volume of the magnetic particles
MAF	Magnetic Abrasive Finishing	χ	Magnetic susceptibility
DC	Direct current	μ_0	permeability of free space
MRR	Material removal rate	H	Magnetic field intensity
K	empirical coefficient	A_{UA}	Amplitude of ultrasonic vibration
F_c	Impact force	ρ	The density of the abrasive slurry
A_c	The contact area between the abrasive particles and the workpiece surface	E	The elastic modulus of the material
Ra	Arithmetical mean deviation	d_4	Geometric parameters associated with the movement trajectory of abrasive particles
ω_r	The angular velocity of the magnetic table	f	The frequency of ultrasonic vibration
δ_{i2}	The displacement amplitude of the abrasive particles over time	A_{i2}	The overall oscillation amplitude of the particles

ACKNOWLEDGEMENT

This work is financially supported by the Hanoi University of Industry (Grant No. DHCN: 46-2024-RD).

REFERENCES

[1] GUO J., et al., 2024, *Internal Surface Finishing and Roughness Measurement: A Critical Review,* Chinese Journal of Aeronautics, 11/17, https://doi.org/10.1016/j.cja.2024.11.013.

[2] YADAV H.N.S., DAS M., 2024, *Advances in Finishing of Optical Complex Substrates: A Comprehensive Review,* Optics & Laser Technology, 176, 110938, https://doi.org/10.1016/j.optlastec.2024.110938.

[3] DEHGHANGHADIKOLAEI A., FOTOVVATI B., MOHAMMADIAN B., NAMDARI N., 2018, *Abrasive Flow Finishing of Stainless Steel 304,* Biomedical Devices, 8/2, 1–8, https://doi.org/10.31031/RDMS.2018.08.000683.

[4] DUY N.T., TIEN D.H., THOA P.T.T., 2022, *A New Environment-Friendly Magnetorheological Finishing and Fuzzy Grey Relation Analysis in Ti-6Al-4V Alloy Polishing*, Manufacturing Rev., 9/17, https://doi.org/10.1051/mfreview/2022013.

[5] TIEN D.H., DUY T.N., THOA P.T.T., 2023, *Applying GPR-FGRA Hybrid Algorithm for Prediction and Optimization of Eco-Friendly Magnetorheological Finishing Ti–6Al–4V Alloy*, International Journal on Interactive Design and Manufacturing, 17/2, 729–745.

[6] DUY TRINH N., et al., 2024, *A Novel Circulating Abrasive Flow Strategy Using Circular Halbach Array for Magneto-Rheological Finishing of Ti-6Al-4V*, Journal of Machine Engineering, 24/1, 118–134, https://doi.org/10.36897/jme/185893.

[7] TIEN D., DUY TRINH N., 2024, *Novel Hybrid Chemical Magnetorheological Fluid for Polishing Ti–6Al–4V Alloy*, Materials and Manufacturing Processes, 39/12, 1–18. https://doi.org/10.1080/10426914.2024.2334674.

[8] YIN S., SHINMURA T., 2004, *A Comparative Study: Polishing Characteristics and its Mechanisms of Three Vibration Modes in Vibration-Assisted Magnetic Abrasive Polishing*, International Journal of Machine Tools and Manufacture, 44/4, 383–390, https://doi.org/10.1016/j.ijmachtools.2003.10.002.

[9] WEI X., YANG X., XIE X., HU W., 2016, *A Material Removal Rate Model-Based Chemical Action of Ultra-Thin SUS304 Substrate in Chemical Mechanical Polishing*, The International Journal of Advanced Manufacturing Technology, 85/1, 287–290, https://doi.org/10.1007/s00170-015-7938-9.

[10] SUN X., ZOU Y., 2017, *Development of Magnetic Abrasive Finishing Combined with Electrolytic Process for Finishing SUS304 Stainless Steel Plane*, The International Journal of Advanced Manufacturing Technology, 92, 3373–3384, https://doi.org/10.1007/s00170-017-0408-9.

[11] CHEN Y., YI J., WANG Z., ZHOU W., DENG H., 2023, *Experimental Study on Ultrasonic-Assisted Electrolyte Plasma Polishing of SUS304 Stainless Steel*, The International Journal of Advanced Manufacturing Technology, 124/7, 2835–2846.

[12] CHEN F., HAO S., MIAO X., YIN S., HUANG S., 2018, *Numerical and Experimental Study on Low-Pressure Abrasive Flow Polishing of Rectangular Microgroove*, Powder Technology, 327, 215–222, https://doi.org/10.1016/j.powtec.2017.12.062.

[13] IM I.-T., MUN S.D., OH S.M., 2009, *Micro Machining of an STS 304 Bar by Magnetic Abrasive Finishing*, Journal of Mechanical Science and Technology, 23/ 7, 1982–1988.

[14] SINGH P., SINGH L., 2014, *Optimization of Magnetic Abrasive Finishing Parameters with Response Surface Methodology*, Proceedings of the International Conference on Research and Innovations in Mechanical Engineering, New Delhi, 2014, 273–286, Springer India.

[15] LEE Y.-H., WU K.-L., JHOU J.-H., TSAI Y.-H, YAN B.-H., 2013, *Two-Dimensional Vibration-Assisted Magnetic Abrasive Finishing of Stainless Steel SUS304*, The International Journal of Advanced Manufacturing Technology, 69, 2723–2733. https://doi.org/10.1007/s00170-013-5242-0.

[16] Gill J.S., Singh L., 2021, *Magnetic Abrasive Polishing of Stainless Steel SS304 with Diamond-Based Sintered Magnetic Abrasives*, Journal of Advanced Manufacturing Systems, 21/04, 797–811, https://doi.org/10.1142/S0219686722500299.

[17] DUY TRINH N., NGUYEN N.T., MINH Q.N., PHAM T.T.T., DUC L.A., 2022, *Application of Magnetic Liquid Slurries and Fuzzy Grey Analysis in Polishing Nickel-Phosphorus Coated SKD11 Steel*, Particulate Science and Technology, 40/4, 401–414, https://doi.org/10.1080/02726351.2021.1948471.

[18] TIEN D.H., DUY T.N., 2024, *Novel Magnetic Field Array Optimization Method for the Chemical Magnetorheological Finishing of Ti-6Al-4V Alloy with SiO_2 Abrasive and Fe3O_4 Magnetic Particles*, The International Journal of Advanced Manufacturing Technology, 134/3, 1395–1417.

[19] RALCHENKO V.G., et al., 2016, *High-Rate Ultrasonic Polishing of Polycrystalline Diamond Films*, Diamond and Related Materials, 66, 171–176. https://doi.org/10.1016/j.diamond.2016.05.002.

[20] MENG F., et al., 2023, *Profile Prediction for Ultrasonic Vibration Polishing of Alumina Ceramics*, International Journal of Mechanical Sciences, 252/15, 108360, https://doi.org/10.1016/j.ijmecsci.2023.108360.

[21] YU T., GUO X., WANG Z., XU P., ZHAO J., 2019, *Effects of the Ultrasonic Vibration Field on Polishing Process of Nickel-Based Alloy Inconel718*, Journal of Materials Processing Technology, 273, 116228, https://doi.org/10.1016/j.jmatprotec.2019.05.009.

[22] HOCHENG H., KUO K.L., 2002, *Fundamental Study of Ultrasonic Polishing of Mold Steel*, International Journal of Machine Tools and Manufacture, 42/1, 7–13, https://doi.org/10.1016/S0890-6955(01)00099-2.

[23] XU Y., WAN Z., ZOU P., ZHANG Q., 2019, *Experimental Study on Chip Shape in Ultrasonic Vibration–Assisted Turning of 304 Austenitic Stainless Steel*, Advances in Mechanical Engineering, 11/8, https://doi.org/10.1177/1687814019870896.

[24] CAO Y., ZHENG L., FAN W., 2022, *An Improved Surface Treatment Process of 304 Stainless Steel Based on Low-Temperature Chromizing and Ultrasonic Vibration Extrusion*, Applied Sciences, 12/22, https://doi.org/10.3390/app122211729.

[25] ZHANG X., WANG J., CHEN J., LYU B., YUAN J., 2024, *Material Removal and Surface Modification of Copper Under Ultrasonic-Assisted Electrochemical Polishing*, Processes, 12/6, https://doi.org/10.3390/pr12061046.

[26] LIU X., WANG J., ZHU J., LIEW P.J., LI C., HUANG C., 2022, *Ultrasonic Abrasive Polishing of Additive Manufactured Parts: An Experimental Study on the Effects of Process Parameters on Polishing Performance*, Advances in Production Engineering & Management, 17/2, 193–204, https://doi.org/10.14743/apem2022.2.430.

[27] LV Z., HUANG C., ZHU H., WANG J., WANG Y., YAO P., 2015, *A Research on Ultrasonic-Assisted Abrasive Waterjet Polishing of Hard-Brittle Materials*, The International Journal of Advanced Manufacturing Technology, 78, 1361–1369, https://doi.org/10.1007/s00170-014-6528-6.

[28] DUY TRINH N., TIEN D., THOA P., QUE N., QUANG K., MAI N., 2024, *Circular Halbach Array Integrated Using an Abrasive Circulating System During the Ultra-Precision Machining of Polymethyl Methacrylate Optical Material*, International Journal of Lightweight Materials and Manufacture, 7/6, 793–808, https://doi.org/10.1016/j.ijlmm.2024.06.007.

[29] YAMAGUCHI H., SSSSS T., SATO T., TANIGUCHI A., TOMURA T., 2006, *Study of Surface Finishing Process Using Magneto-Rheological Fluid (MRF)*, Journal of the Japan Society for Precision Engineering, Contributed Papers, 72, 100–105.

[30] MISRA A., PANDEY P.M., DIXIT U.S., 2017, *Modeling of Material Removal in Ultrasonic Assisted Magnetic Abrasive Finishing Process*, International Journal of Mechanical Sciences, 131–132, 853–867, https://doi.org/10.1016/j.ijmecsci.2017.07.023.

[31] SHUKLA V.C., PANDEY P.M., DIXIT U.S., ROY A., SILBERSCHMIDT V., 2017, *Modeling of Normal Force and Finishing Torque Considering Shearing and Ploughing Effects in Ultrasonic Assisted Magnetic Abrasive Finishing Process with Sintered Magnetic Abrasive Powder*, Wear, 390–391, 11–22, https://doi.org/10.1016/j.wear.2017.06.017.

[32] KHALAJ AMINEH S., FADAEI TEHRANI A., MOSADDEGH P., MOHAMMADI A., 2015, *A Comprehensive Experimental Study on Finishing Aluminum Tube by Proposed UAMAF Process*, Materials and Manufacturing Processes, 30/1, 93–98, https://doi.org/10.1080/10426914.2014.965319.

[33] MULIK R.S., PANDEY P.M., 2011, *Ultrasonic Assisted Magnetic Abrasive Finishing of Hardened AlSi 52100 Steel Using Unbonded Sic Abrasives*, International Journal of Refractory Metals and Hard Materials, 29/1, 68–77, https://doi.org/10.1016/j.ijrmhm.2010.08.002.

[34] ZHOU K., CHEN Y., DU Z.W., NIU F.L., 2015, *Surface Integrity of Titanium Part by Ultrasonic Magnetic Abrasive Finishing*, The International Journal of Advanced Manufacturing Technology, 80/5, 997–1005, https://doi.org/10.1007/s00170-015-7028-z.

[35] MISRA A., PANDEY P.M., DIXIT U.S., 2017, *Modeling and Simulation of Surface Roughness in Ultrasonic Assisted Magnetic Abrasive Finishing Process*, International Journal of Mechanical Sciences, 133, 344–356, https://doi.org/10.1016/j.ijmecsci.2017.08.056.

[36] SUN X., ZOU Y., 2018, *Study on Electrolytic Magnetic Abrasive Finishing for Finishing Stainless Steel SUS304 Plane with a Special Compound Machining Tool*, Journal of Manufacturing and Materials Processing, 2/3, 41, https://doi.org/10.3390/jmmp2030041.

[37] MISRA A., PANDEY P.M., DIXIT U.S., ROY A., SILBERSCHMIDT V.V., 2017, *Modeling of Finishing Force and Torque in Ultrasonic-Assisted Magnetic Abrasive Finishing Process*, Proceedings of the Institution of Mechanical Engineers, Part B: Journal of Engineering Manufacture, 233/2, 411–425, https://doi.org/10.1177/0954405417737579.

[38] JAYAWANT B.V., SINHA P.K., AYLWIN D.G., 1976, *Feedback Control Systems for D.C. Electromagnets in Passenger-Carrying Vehicles*, International Journal of Control, 24/5, 627–639.

[39] NEYMAN V.Y., NEYMAN L.A., PETROVA A.A., 2008, *Calculation of Efficiency of a DC Power Electromagnet for Mechanotronic Systems*, 2008 Third International Forum on Strategic Technologies, 452–454, https://doi.org/10.1109/IFOST.2008.4602851.

[40] DUAN Y., IONEL D.M., 2013, *A Review of Recent Developments in Electrical Machine Design Optimization Methods with a Permanent-Magnet Synchronous Motor Benchmark Study*, IEEE Transactions on Industry Applications, 49/3, 1268–1275, https://doi.org/10.1109/TIA.2013.2252597.

[41] XUAN T., LI J., LI B., FAN W., 2021, *Effects of the Non-Uniform Magnetic Field on the Shear Stress and the Microstructure of Magnetorheological Fluid*, Journal of Magnetism and Magnetic Materials, 535, 168066, https://doi.org/10.1016/j.jmmm.2021.168066.

[42] SHEIKHOLESLAMI M., RASHIDI M.M., GANJI D.D., 2015, *Effect of Non-Uniform Magnetic Field on Forced Convection Heat Transfer of Fe_3O_4–Water Nanofluid*, Computer Methods in Applied Mechanics and Engineering, 294, 299–312, https://doi.org/10.1016/j.cma.2015.06.010.

[43] KIM B.C., JEON S.B., MOON J.I., KIM S.M., KIM S.W., CHO I.K., 2016, *A Method of Evaluating Magnetic Field Strength by Correction Between Uniform and Non-Uniform Field in Near-Field*, IEEE Global Electromagnetic Compatibility Conference (GEMCCON), 1–3, https://doi.org/10.1109/GEMCCON.2016.7797319.

[44] XIAO Y., ZHENG J., CHEN S., 2024, *Study on the Static Normal Force of MRF in Non-Uniform Magnetic Field*, Journal of Magnetism and Magnetic Materials, 599, 172063, https://doi.org/10.1016/j.jmmm.2024.172063.
[45] JHA S., JAIN V.K., 2004, *Design and Development of the Magnetorheological Abrasive Flow Finishing (MRAFF) Process*, International Journal of Machine Tools and Manufacture, 44/10, 1019–1029, https://doi.org/10.1016/j.ijmachtools.2004.03.007.
[46] ANJANEYULU K., VENKATESH G., 2021, *Optimization of Process Parameters of Magnetic Abrasive Finishing Using Jaya Algorithm*, Materials Today: Proceedings, 41/5, 1035–1040, https://doi.org/10.1016/j.matpr.2020.06.568.
[47] YU T., WANG Z., GUO X., XU P., ZHAO J., CHEN L., 2019, *Effect of Ultrasonic Vibration on Polishing Monocrystalline Silicon: Surface Quality and Material Removal Rate*, The International Journal of Advanced Manufacturing Technology, 103/5, 2109–2119, https://doi.org/10.1007/s00170-019-03385-y.
[48] AHMAD S., SINGARI R.M., MISHRA R.S., 2020, *Modelling and Optimisation of Magnetic Abrasive Finishing Process Based on a Non-Orthogonal Array with ANN-GA Approach*, Transactions of the IMF, 98/4, 186–198, https://doi.org/10.1080/00202967.2020.1776966.
[49] MULIK R.S., PANDEY P.M., 2012, *Experimental Investigations and Modeling of Finishing Force and Torque in Ultrasonic Assisted Magnetic Abrasive Finishing*, Journal of Manufacturing Science and Engineering, 134/5, https://doi.org/10.1115/1.4007131.
[50] WANG L., SUN Y., CHEN F., ZHANG G., SUN Y., ZUO D., 2023, *Modeling and Simulation of the Action Mechanism of Multi-Particles in Magnetic Abrasive Finishing for Internal Blind Cavity Using the Discrete Element Method*, The International Journal of Advanced Manufacturing Technology, 125/3, 1179–1192.